Structural and Gas-Sensing Properties of WO_3 Nanocrystalline Powders Obtained by a Sol-Gel Method From Tungstic Acid

Ismael Jiménez, Jordi Arbiol, Albert Cornet, and Joan Ramon Morante

***Abstract*—WO_3 nanocrystalline powders were obtained from tungstic acid following a sol-gel process. Evolution of structural properties with annealing temperature was studied by X-ray diffraction and Raman spectroscopy. These structural properties were compared with those of WO_3 nanopowders obtained by the most common process of pyrolysis of ammonium paratungstate, usually used in gas sensors applications. Sol-gel WO_3 showed a high sensor response to NO_2 and low response to CO and CH_4. The response of these sensor devices was compared with that of WO_3 obtained from pyrolysis, showing the latter a worse sensor response to NO_2. Influence of operating temperature, humidity, and film thickness on NO_2 detection was studied in order to improve the sensing conditions to this gas.**

***Index Terms*—Gas sensor device, nanoparticles, preparation, structural characterization, WO_3.**

I. Introduction

NOWADAYS, WO_3 is an appreciated material in different applications like solar cells [1], [2], catalysis [3], [4], electrochromic devices [5], [6], and gas sensors [7], [8]. Many methods have been applied to obtain thin films of this material such as sputtering [9], CVD [10], spray-pyrolysis [11], and spin coating or dip coating of sol-gel precursors [12].

On the other hand, some applications in the field of gas sensors often use nanopowders. These devices are usually operated at temperatures ranging from 200 to 400 °C so the material has to be thermally stabilized at higher temperatures. After this annealing, they are implemented as a sensitive layer. One of the most used routes to obtain WO_3 nanopowders is the pyrolysis of ammonium paratungstate [13], [14]. It has been shown that this route is able to obtain WO_3 with nanometric grain size, and it is a well-known technique in the field of gas sensors. However, its preparation needs using nitric acid and it can lead to contamination of samples if it is not removed at the right step of preparation.

In this paper, we present nanocrystalline WO_3 powder obtained by a sol-gel process from dissolution of tungstic acid in a mixture of methanol/water, which is a route that has been scarcely used in catalysis [15]. Besides, no complete study about influence of annealing on structural properties and grain growth has been presented and this route has never been applied to gas sensors, as far as we know. This method presents the advantage of being cleaner than the pyrolytic route and no filtration is needed. Dried gels were characterized by Raman spectroscopy and X-ray diffraction (XRD) to determine its nature. Nanocrystalline powders were obtained by annealing of dried gels and they were characterized by transmission electron microscopy (TEM), XRD, and Raman. These structural characteristics were compared with those of WO_3 obtained by the pyrolysis of ammonium paratungstate. Finally, sensitive layers were obtained from these nanopowders and the performance of the obtained gas sensor devices was studied in CO, CH_4, and NO_2 atmospheres.

Manuscript received September 30, 2001; revised January 22, 2002. This paper was presented at the Matchems Workshop, Brescia, Italy, September 13th–14th, 2001. The associate editor coordinating the review of this paper and approving it for publication was Dr. Eugenii Katz.

The authors are with the Enginyeria i Materials Electrònics, Departament d'Electrònica, Universitat de Barcelona, Barcelona, Spain (e-mail: ijimenez@el.ub.es; arbiol@el.ub.es; cornet@el.ub.es; morante@el.ub.es).

Digital Object Identifier 10.1109/JSEN.2002.803747

II. Experimental

WO_3 nanocrystalline powders were obtained following a sol-gel route using tungstic acid as a precursor. Tungstic acid was dissolved in a mixture of methanol and water with a molar ratio of 25. This solution was heated at 80 °C for 24 h under stirring in air. Afterwards, it was dried by further heating at 110 °C in air. Dried gels were calcined in a furnace at 400, 500, 600, and 700 °C for 5 h to obtain nanocrystalline WO_3.

In order to compare the structural properties of this sol-gel WO_3 with the properties of the WO_3 obtained from pyrolysis of ammonium paratungstate, a series of samples of WO_3 were also obtained by the latter route. First, ammonium paratungstate was dissolved in water (2.5% in weight). It was gently stirred for 2 h at room temperature. A nitric acid solution (20% in weight) was slowly added to the previous solution of ammonium paratungstate and this was heated at 80 °C for 20 h. The dissolution was filtrated to remove nitric acid and then dried at 120 °C for 8 h. The resulting material was calcined in a furnace at 400, 500, 600, and 700 °C for 5 h to obtain nanocrystalline WO_3.

XRD patterns of the nanopowders were obtained with a Siemens D-500 X-ray diffractometer using Cu–Kα radiation, with operating voltage of 40 kV and current of 30 mA. Raman scattering measurements were obtained in backscattering geometry with a Jobin–Yvon T64000 spectrometer coupled to an Olympus metallographic microscope. Excitation was provided by an argon–ion laser operating at a wavelength of 488.0 or 457.5 nm with a low incident power to avoid thermal effects. Raman shifts were corrected by using silicon reference spectra after each measurement. Transmission electron microscopy

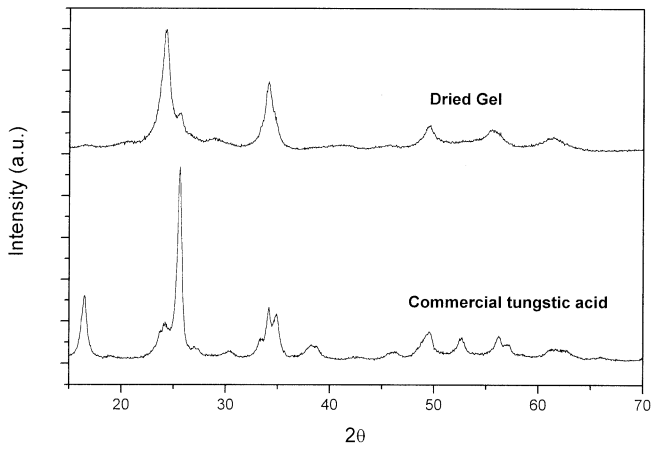

Fig. 1. Comparison of the XRD spectra of commercial tungstic acid and dried gel obtained.

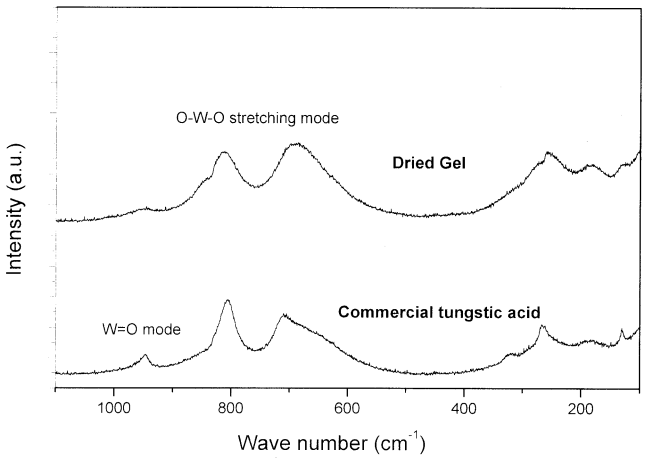

Fig. 2. Comparison of the Raman spectra of commercial tungstic acid and dried gel obtained.

(TEM) was carried out on a Phillips CM30 SuperTwin electron microscope operated at 300 keV with 0.19 nm point resolution. For TEM observations, WO_3 nanopowders were ultrasonically dispersed in ethanol and deposited on amorphous holey carbon membranes.

Sensitive films were deposited by pulverization coating [16] of annealed nanopowders over alumina substrates with interdigited Pt electrodes. These substrates also had a Pt heater on the backside for self-heating. Sensing films had a thickness of a few microns to have sensor resistance in the range of kΩ to MΩ in air. These gas sensor devices were placed in a stainless steel test chamber where a controlled atmosphere was provided by means of mass flow controllers. The same computer, using acquisition boards, acquired the response of the sensors to different concentrations of CO, CH_4, and NO_2 in synthetic air.

III. Results and Discussion

A. Structural Characterization

Dried gels were obtained after heating the dissolution of tungstic acid in methanol and water at 80 °C and evaporate the solvent at 110 °C. These dried gels were characterized by XRD and Raman. In Fig. 1, XRD spectra of commercial tungstic acid and these dried gels are compared. Dried gels present a main peak at $2\theta = 24.2°$. This corresponds to the peak (200) of WO_3 in triclinic structure (JCPDS card 20-1323). Crystalline WO_3 presents a pseudocubic structure with a slight distortion of the cubic ReO_3-type lattice, being monoclinic and triclinic the most common structures at ambient temperature [17], although it appears that it is really triclinic WO_3 that is the equilibrium form at ambient pressure and temperature. However, it is interesting to notice that dried gels still present small peaks at $2\theta = 16.5°$ and $2\theta = 25.6°$. Although these peaks are also present in tungstic acid, tungsten oxide hydrates ($WO_3 \cdot nH_2O$) present main peaks at $2\theta = 16.5°$ and $2\theta = 25.7°$ (JCPDS card 43-0679). It seems more reasonable to assign these signals of dried gels to tungsten oxide hydrate, which is an intermediate product between tungstic acid and tungsten oxide [15]. Therefore, dried gels should be identified as WO_3 with a small amount of $WO_3 \cdot nH_2O$.

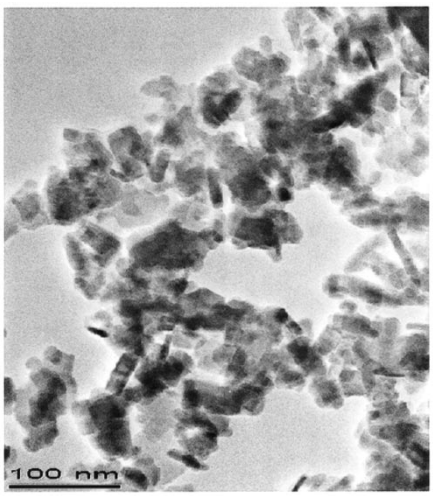

Fig. 3. General TEM view of WO_3 nanoparticles annealed at 400 °C for 5 h.

Raman spectroscopy was used to confirm XRD results. Fig. 2 presents a comparison of the Raman spectra of commercial tungstic acid and dried gel. Tungstic acid has its main peaks at 806 and 710 cm^{-1}. These peaks are shifted to 812 and 700 cm^{-1} for the dried gel. These bands are well identified as belonging to the stretching mode O–W–O, which in monocrystalline WO_3 are present at 807 and 715 cm^{-1} [17]. However, the peak at 947 cm^{-1}, that is present in commercial tungstic acid, has not completely disappeared in dried gel. This peak is reported to correspond to the mode W = O, which is also a bond of tungsten oxide hydrates ($WO_3 \cdot nH_2O$) when a water molecule occupies one axial position [12], [17]. This confirms the XRD result about that some tungsten oxide hydrate was present. However, the presence of structural water should be taken into account as it has been reported to be present in this stage [15] and it could be the responsible for the shift in the Raman peaks due to lattice distortion.

Dried gels were calcined to obtain nanocrystalline WO_3. They were annealed for 5 h at 400, 500, 600, and 700 °C in air, in order to monitor the evolution of strucutral characteristics with annealing temperature. Fig. 3 shows a TEM micrograph of

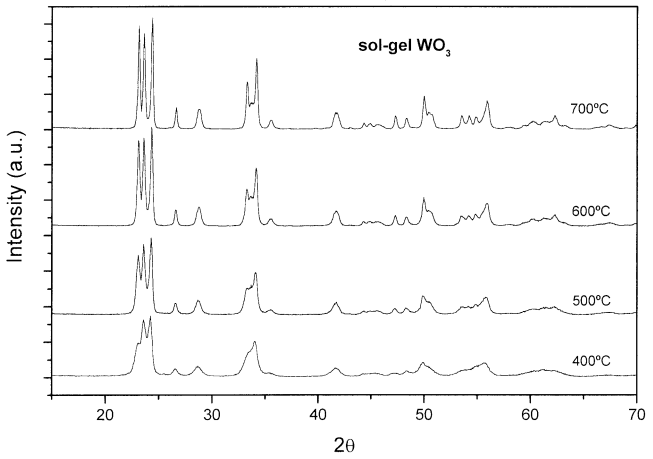

Fig. 4. Evolution with annealing temperature of the XRD spectra of the sol-gel WO_3.

a WO_3 grain annealed at 400 °C. It can be seen that particles are in the nanometric range. However, their size distribution was not homogeneous, especially at low annealing temperatures, where big particles coexisted with smaller ones. Fig. 4 shows the XRD spectra of the annealed nanopowders. Main peaks were found at $2\theta = 23.0°$, 23.6°, and 24.3°, which are identified as corresponding to Miller index (002), (020), and (200), respectively, in triclinic WO_3. Therefore, crystalline WO_3 was obtained after calcination of gels at 400 °C for 5 h. Annealing at 300 °C for 5 h or at 400 °C for 2 h lead to amorphous WO_3. No trace of tungsten oxide hydrate was found after this annealing. Using Scherrer's equation [18], average crystallite size of WO_3 was estimated from XRD spectra averaging results from the three main crystallographic directions, with an error lower than 5 nm. Values for each annealing temperature are shown in Table I. As it was expected, an increase in annealing temperature leads to grain growth. However, this value has to be taken as an estimation of the grain size average as TEM images show a dispersion in grain size and in reported works about gas sensors based on WO_3 powders, sensor particles are on the range 100–1000 nm [19]. In this case, grain diameter ranged from 27 nm for powder annealed at 400 °C to 68 nm for the one annealed at 700 °C (Table I).

WO_3 powders were also obtained by the well-known method of pyrolysis applied to ammonia paratungstate. As explained before, ammonium paratungstate was dissolved in water and a dissolution of nitric acid was slowly added. After heating at 80 °C for 20 h, the remaining dissolution was filtrated and the solid was further heated at 120 °C for 8 h. This material was also annealed at 400, 500, 600, 700 °C for 5 h in air in order to compare both kinds of WO_3 annealed under the same conditions. Fig. 5 shows XRD spectra corresponding to WO_3 obtained from ammonium paratungstate after annealing at 700 °C, compared with sol-gel WO_3 annealed at the same temperature. JCPDS card 20-1323 values for crystalline WO_3 are also shown. It can be seen that it has the same structure as previous sol-gel WO_3 but, in this case, reflection corresponding to (002) had the higher intensity, which does not fully agree with relative intensities commonly reported. This can be due to intrinsic defects due to the displacement of tungsten from the center of its octahedron and the tilting of the WO_6 octahedra. Therefore, WO_3 obtained by the sol-gel process had structural properties closer to those of crystalline WO_3. Crystalline size was also estimated by Scherrer's equation (see Table I) and it had similar values than those obtained by the sol-gel process. These values agree with those reported for WO_3 obtained by pyrolysis [14].

Raman spectra of both series of annealed samples were also analyzed. Fig. 6 shows the evolution of sol-gel WO_3 nanopowders with annealing temperature. It can be seen that sol-gel WO_3 present typical structure for crystalline WO_3, with three main regions at 900–600, 400–200, and below 200 cm^{-1}. It has been established that they correspond, respectively, to stretching, bending and lattice modes. This great number of active modes is due to the distortion of the ReO_3-type structure in real monoclinic situation, as group theory shows that this structure should only have two active modes [20]. It has to be remarked that no signal of W = O bond was found, what means that any trace of water in dried gels was eliminated. Some other techniques as spray pyrolysis or vacuum evaporation of powder have failed in achieving WO_3 free of water, according to their Raman results [11], [21].

Similar spectra were found for samples obtained by the pyrolytic process. Characteristics of the main Raman peak such as position and FWHM are presented for both series of samples in Fig. 7. It can be seen that FWHM decreases with annealing temperatures, which was expected as annealing at higher temperatures must lead to a decrease in lattice defects and therefore peaks must narrow. On the other hand, evolution of peak position with temperature is not so straightforward. For sol-gel WO_3, peak position is close to that usually found in the literature (807 cm^{-1}) and it approaches this value as annealing temperature increases. Similar behavior has already been reported for other sol-gel processes [12]. However, pyrolytic WO_3 has its main peak shifted from the common position and it does not move to the common value as annealing temperature increases. This could be a sign of a more distorted lattice and could explain the difference in relative intensity of XRD signals presented before. Similar differences in Raman shift have been reported, probably due to the presence of water according to its Raman spectra. However, in our case, WO_3 obtained by pyrolysis did not show any trace of water after annealing.

Therefore, the sol-gel process has been able to obtain WO_3 nanocrystalline powders with better structural properties than those obtained by pyrolysis of ammonium paratungstate. Powders annealed at 400 °C for 5 h appear to be already crystalline. Control of grain growth is possible by varying the temperature of annealing and its values are similar to those obtained by pyrolysis.

B. Sensor Devices: Gas-Sensing Properties

Since WO_3 annealed at 400 °C was already crystalline and it has the smaller grain size, it was chosen as the best candidate as sensing element. It has been extensively reported that small grain sizes and high surface areas lead to better response to gases for gas sensors based on metal oxides. As interactions are surface processes, more surface sites for reaction are available respect to the bulk when grain size decreases. However,

TABLE I
EVOLUTION WITH ANNEALING TEMPERATURE OF THE GRAIN SIZE AVERAGED FROM XRD DATA FOR PYROLYTIC AND SOL-GEL WO_3

Annealing Temperature (°C)	Grain size of sol-gel WO_3 (nm)	Grain size of pyrolytic WO_3 (nm)
400	27	27
500	37	38
600	53	50
700	68	69

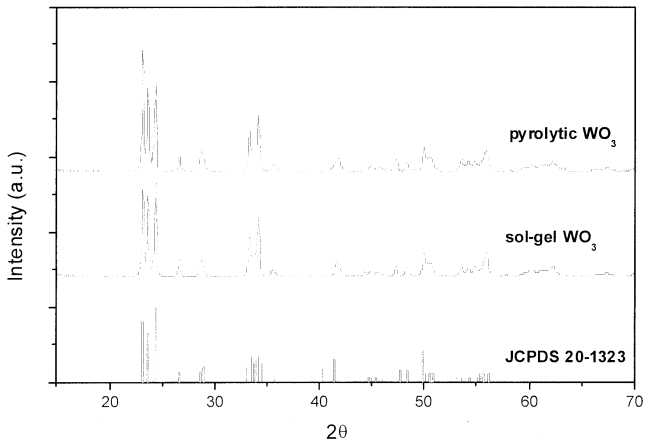

Fig. 5. Comparison of the XRD spectra of nanocrystalline WO_3 powders obtained by pyrolysis and sol-gel annealed at 700 °C with the card JCPDS 20-1323.

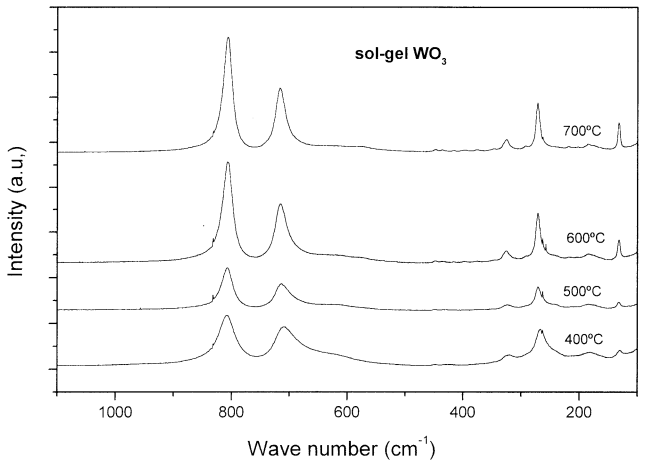

Fig. 6. Evolution with annealing temperature of the Raman spectra of the sol-gel WO_3.

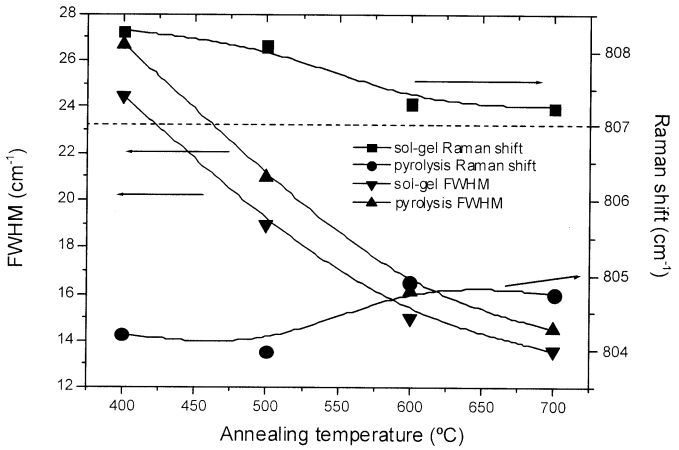

Fig. 7. Comparison of the evolution with annealing temperature of the FWHM and Raman shift of the main vibration mode of the pyrolytic and sol-gel WO_3.

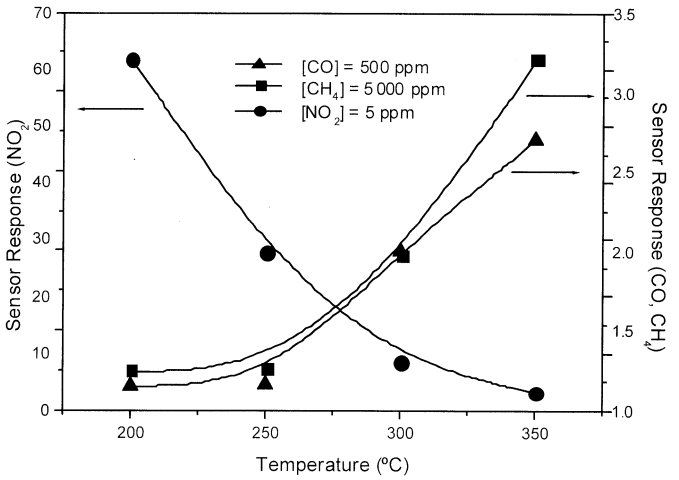

Fig. 8. Response of the gas-sensor devices based on sol- gel WO_3 as a function of operating temperature to 5 ppm of NO_2, 500 ppm of CO, and 5000 ppm of CH_4 in dry air.

the sensing material has to be previously annealed at high temperatures, which increases grain size, to avoid drift in sensor response due to structural changes of the sensitive layer. Therefore, a compromise between stability and sensor response must be reached.

Sensor response to CO, CH_4, and NO_2 was evaluated in the temperature range from 200 to 350 °C. Since sensor resistance decreased in the presence of CO and CH_4 and increased in the presence of NO_2, sensor response was evaluated as R_{AIR}/R_{GAS} for CO and CH_4 and as R_{GAS}/R_{AIR} for NO_2. Fig. 8 shows that sensor response to CO and CH_4 increases when operating temperature is increased in this range, while response to NO_2 has an opposite behavior. CO and CH_4 react with chemisorbed oxygen, which has previously captured electrons from the conduction band. After the reaction, these electrons return to the conduction band so conductivity increases. As these reactions are thermally activated, sensor response is improved when operating temperature is increased in the range of temperatures studied. On the other hand, NO_2 is chemisorbed on the surface of nanoparticles, captures electrons and makes the conductivity decrease. Desorption of these molecules increases when temperature is raised and therefore sensor response to NO_2 increases when operating temperature decreases. While sensor response to 5 ppm of NO_2 was over

60 at 200 °C, it was only around 3 for 500 ppm of CO or 5000 ppm of CH_4 at 350 °C.

One of the remarkable features of WO_3 in gas sensing applications is its high sensor response to NO_2 and its low response to gases like CO and CH_4, specially if it is compared with the most used SnO_2, that usually has better performances in CO and CH_4 detection. This makes WO_3 an interesting material for NO_2 detection avoiding significance interferences from CO or CH_4 [22]. Although a completely satisfactory answer to this different behavior between these oxides has not been given yet, the different role played by oxygen vacancies seem to be the responsible for this different behavior. In tin oxide, oxygen vacancies can be found as intrinsic point defects present in the lattice or at grain boundaries [23] and a diffusion of these vacancies between the surface and the bulk is possible [24]. It has been shown in [25] that in tin oxide, the active oxygen species is probably O_2^- and its correct formulation is an oxygen molecule adsorbed in or on an oxygen vacancy. This species is highly reactive with gases like CO or CH_4. On the other hand, oxygen vacancies have a completely different behavior in WO_3. In this compound, point defects like oxygen vacancies are largely eliminated by the formation of crystallographic shear phases [26]. In tungsten oxide, it is possible to shear the structure in such a way that the vacancies are eliminated and tungsten atoms remain more closely spaced, so pairs of W^{5+} atoms would be found to compensate the charge of the oxygen that leaves the vacancy. This was confirmed in our samples by electron paramagnetic resonance (EPR) as no trace of paramagnetic W^{5+} signal was found. While isolated W^{5+} species are paramagnetic, pairs of these atoms are diamagnetic and so EPR silent. In this situation, it would be reasonable to think that adsorption of oxygen molecules could not be done by the same mechanism of SnO_2, which would explain the low response of WO_3 to CO and CH_4. On the other hand, W^{5+} atoms could be assigned as a chemisorption site for NO_2 detection since In^{2+} and Mo^{5+} have been assigned like this in In_2O_3 and MoO_3, respectively [27].

Sensor response to NO_2 was analyzed in more detail as WO_3 showed to have a good response to this gas. The best operation temperature was fixed at 250 °C because sensor response decreased at higher temperatures and response and recovery times were too slow (more than one minute) at lower temperatures. Sensor response was monitored at different concentrations of NO_2 (0.5, 1, and 2 ppm) at two different humidity conditions (dry air and 50% of relative humidity). Sensor response of WO_3 annealed at 400 °C, both sol-gel and pyrolytic routes, is shown in Fig. 9. It can be seen that in both conditions of humidity, sensor response of WO_3 obtained by the sol-gel route is better than that of tungsten oxide obtained from pyrolysis. As grain sizes were nearly the same, this difference is surely due to the differences in structural properties previously presented. This confirms that the followed route is not only able to obtain a material with better crystalline properties but also gives a better sensor response to NO_2. It is also remarkable that the influence of water on sensor response is greater on sensors based on WO_3 obtained from the pyrolytic route, being greater at a relative humidity of 50% than in dry air. Besides, if sensor response (S) is fitted using a function $S = A * C^z$, where C is the gas concentration of NO_2, which is proportional to the partial gas pressure,

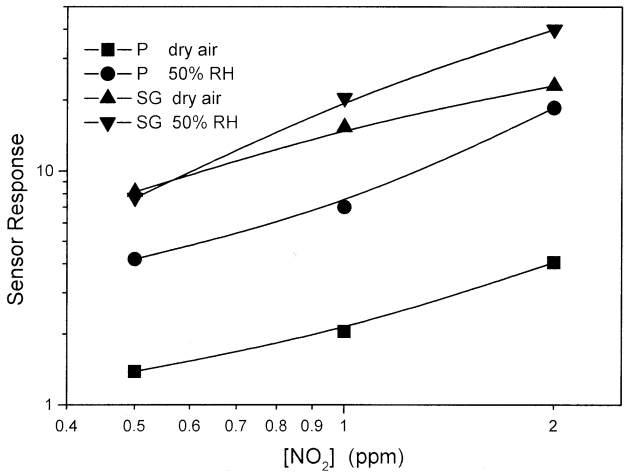

Fig. 9. Comparison of the response of sol-gel (SG) and pyrolytic (P) WO_3 to 0.5, 1, and 2 ppm of NO_2 in dry and humidified air (50% of relative humidity). Operating temperature was fixed at 250 °C.

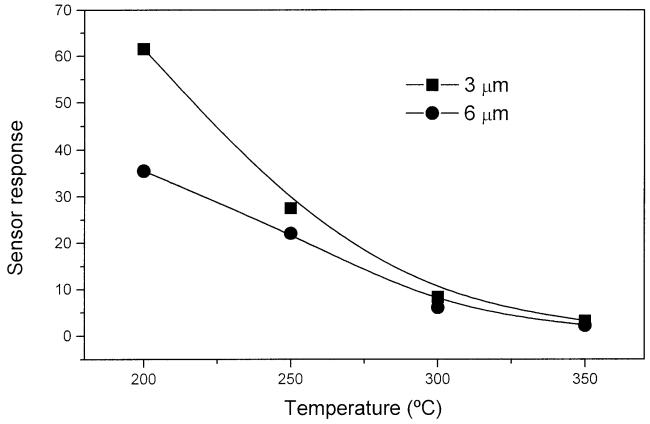

Fig. 10. Comparison of the evolution sensor response with operating temperature of 3- and 6-μm-thick sensitive layer to 5 ppm of NO_2.

it is found that exponent z depends on humidity. In dry air, its value is 0.7 for sol-gel WO_3 and 0.8 for pyrolytic WO_3, while at a relative humidity of 50% its value increases to 1.1 for both materials. Although theoretical models account for a value of 1 for exponent z if the interaction is made by NO_2^- species [30], it has been shown that this parameter is highly dependent on the microstructure of the film, especially in thick-film gas sensors [28]. One accepted mechanism of interaction between water and tin oxide, which has been deeply studied, involves the binding of a hydroxyl group to a tin atom of the lattice and the formation of an oxygen vacancy [29]. If this mechanism worked for tungsten oxide, an oxygen vacancy would lead to the formation of a pair of W^{5+} by the mechanism explained before. This would lead to more reaction sites for NO_2 and would explain the increase in sensor response for NO_2 when relative humidity is at 50%. Nevertheless, spectroscopic measurements should be carried on WO_3 to confirm this hypothesis.

Finally, microstructure effects on sensor response to NO_2 where evaluated by testing sensors with two different sensitive layer thickness (3 and 6 μm). Results are shown in Fig. 10. It was found that the thinner layer was more sensitive to NO_2 and the effect is clearer at lower temperatures. Similar results were

found for gas sensors based on SnO_2 [16] where the sensitive layer was obtained using the same deposition technique. It was attributed to the fact that sensitive films obtained by pulverization coating have a higher surface area when the thickness is reduced from 6 to 3 μm. Therefore, more sites for reaction of the NO_2 molecule are available respect to the bulk layer.

IV. Conclusion

It was found that nanocrystalline WO_3 powders can be obtained from tungstic acid by a sol-gel route. Dried gels were identified as WO_3 with a small amount water, either structural or as tungsten oxide hydrate. Crystallization was found after annealing at 400 °C. Grain growth was controlled by annealing conditions. Structural properties were close to those reported for monocrystalline WO_3, while nanopowders obtained by the well-known method of pyrolysis of ammonium paratungstate had some lattice distortions according to XRD and Raman results. Sol-gel material appeared to be suitable for NO_2 sensing applications at 250 °C, with a low sensor response to CO and CH_4. Its sensor response to NO_2 was better than that of pyrolytic WO_3 under the same conditions due to differences in structural properties. Humidity affected NO_2 detection by varying the chemisorptions sites, although its influence was greater on pyrolytic WO_3. It was also shown that a film thickness of 3 μm showed a better sensor response to NO_2 than that of a film of 6-μm thickness due to the nature of NO_2 interaction.

References

[1] J. P. Cronin, D. J. Tarico, J. C. L. Tonazzi, A. Agrwal, and S. R. Kennedy, "Microstructure and properties of sol-gel deposited WO_3 coatings for large are electrochromic windows," *Sol. Energy Mater. Sol. C*, vol. 29, pp. 371–386, 1993.

[2] A. T. Baker, S. G. Bosi, J. M. Bell, D. R. MacFarlane, B. G. Monsma, I. Skryabin, and J. Wang, "Degradation mechanisms in electrochromic devices based in sol-gel deposited thin films," *Sol. Energy Mater. Sol. C*, vol. 39, pp. 133–143, 1995.

[3] M. Najbar, E. Broclawik, A. Góra, J. Camra, A. Bialas, and A. Weselucha-Birczynska, "Evolution of the surface species of the V_2O_5–WO_3 catalysts," *Chem. Phys. Lett.*, vol. 325, pp. 330–339, 2000.

[4] M. A. Reiche, P. Hug, and A. Baiker, "Effect of grafting sequence on the behavior of titania-supported V_2O_5–WO_3 catalysts in the selective reduction of NO by NH_3," *J. Catal.*, vol. 192, pp. 400–411, 2000.

[5] L. Su and Z. Lu, "All solid state smart window of electrocdeposited WO_3 and TiO_2 particulate film with ptrefg gel electrolyte," *J. Phys. Chem. Solids*, vol. 59, pp. 1175–1180, 1998.

[6] P. Bonhôte, E. Gogniat, M. Grätzel, and P. V. Ashrit, "Novel electrochromic devices on complementary nanocrystalline TiO_2 and WO_3 thin films," *Thin Solid Films*, vol. 350, pp. 269–275, 1999.

[7] C. Cantalini, W. Wlodarski, Y. Li, M. Passacantando, S. Santucci, E. Comini, G. Faglia, and G. Sberveglieri, "Investigation on the O_3 sensitivity properties of WO_3 thin films prepared by sol-gel, thermal evaporation and r.f. sputtering techniques," *Sens. Actuators B*, vol. 64, pp. 182–188, 2000.

[8] X. Wang, N. Miura, and N. Yamazoe, "Study of WO_3-based sensing materials for NH_3 and NO detection," *Sens. Actuators B*, vol. 66, pp. 74–76, 2000.

[9] I. Ruokamo, T. Kärkkäinen, J. Huusko, T. Ruokanen, M. Blomberg, H. Torvela, and V. Lantto, "H_2S response of WO_3 thin-film sensors manufactured by silicon processing technology," *Sens. Actuators B*, vol. 18-19, pp. 486–488, 1994.

[10] C. Cantalini, M. Pelino, H. T. Sun, M. Faccio, S. Santucci, L. Lozzi, and M. Passacantando, "Cross sensitivity and stability of NO_2 sensors from WO_3 thin film," *Sens. Actuators B*, vol. 35-36, pp. 112–118, 1996.

[11] M. Regragui, M. Addou, A. Outzourhit, J. C. Bernédé, Elb. El Idrissi, E. Benseddik, and A. Kachouane, "Preparation and characterization of pyrolytic spray deposited electrochromic tungsten trioxide films," *Thin Solid Films*, vol. 358, pp. 40–45, 2000.

[12] A. Takase and K. Miyakawa, "Raman Study on sol-gel derived tungsten oxide from tungsten ethoxide," *Jpn. J. Appl. Phys.*, vol. 30, pp. L 1508–1511, 1991.

[13] M. Akiyama, J. Tamaki, N. Miura, and N. Yamazoe, "Tungsten oxide-based semiconductor sensor highly sensitive to NO and NO_2," *Chem. Lett.*, pp. 1611–1614, 1991.

[14] J. Tamaki, Z. Zhang, K. Fujimori, M. Akiyama, T. Harada, N. Miura, and N. Yamazoe, "Grain-size effects in tungsten oxide-based sensor for nitrogen oxides," *J. Electrochem. Soc.*, vol. 141, pp. 2207–2210, 1994.

[15] J. H. Kim and K. L. Kim, "A study of preparation of tungsten nitride catalysts with high surface area," *Appl. Catal. A*, vol. 181, pp. 103–111, 1999.

[16] I. Jiménez, A. Cirera, J. Folch, A. Cornet, and J. R. Morante, "Innovative method of pulverization coating of prestabilized nanopowders for mass production of gas sensors," *Sens. Actuators B*, vol. 78, pp. 78–82, 2001.

[17] M. F. Daniel, B. Desbat, J. C. Lassegues, B. Gerand, and M. Figlarz, "Infrared and Raman study of WO_3 tungsten trioxides and WO_3,xH_2O tungsten trioxides hydrates," *J. Solid State Chem.*, vol. 67, pp. 235–247, 1987.

[18] P. Scherrer, *Gôttinger Nachr.*, 1918, vol. 2, p. 98.

[19] S. R. Aliwell, J. F. Halsall, K. F. E. Pratt, J. O'Sullivan, R. L. Jones, R. A. Cox, S. R. Utembe, G. M. Hansford, and D. E. Williams, "Ozone sensors based on WO_3: A model for sensor drift and a measurement correction method," *Meas. Sci. Technol.*, vol. 12, pp. 684–690, 2001.

[20] E. Salje, *Acta Crystallogr. Sect. A: Crysta. Phys., Diffr., Theor. Gen. Crystallogr.*, 1975, vol. 31, p. 360.

[21] Y. A. Yang, Y. W. Cao, P. Chen, B. H. Loo, and J. N. Yao, "Microstuctural properties of an electrochromic WO_3 thin film," *J. Phys. Chem. Solids*, vol. 59, pp. 1667–1670, 1998.

[22] C. Cantalini, H. T. Sun, M. Faccio, M. Pellino, S. Santucci, L. Lozzi, and M. Passacantando, "NO_2 sensitivity of WO_3 thin film obtained by high vacuum thermal evaporation," *Sens. Actuators B*, vol. 31, pp. 81–87, 1996.

[23] D. G. Rickerby, M. C. Horrillo, J. P. Santos, and P. Serrini, "Microstructural characterization of nanograin tin oxide gas sensors," *NanoStruc. Mater.*, vol. 9, pp. 43–52, 1997.

[24] D. Kohl, "The role of noble metals in the chemistry of solid-state gas sensors," *Sens. Actuators, B*, vol. 1, pp. 158–165, 1990.

[25] D. E. Williams and K. F. E. Pratt, "Classification of reactives sites on the surface of polycrystalline tin dioxide," *J. Chem. Soc. Faraday Trans.*, vol. 94, pp. 3493–3500, 1998.

[26] R. J. D. Tilley, *Deffect Crystal Chemistry*. Glasgow, U.K.: Blackie, 1987.

[27] M. Ivanovskaya, A. Gurlo, and P. Bogdanov, "On the role of catalytic additives in gas-sensitivity of SnO_2–Mo based thin film sensors," *Sens. Actuators B*, vol. 77, pp. 264–267, 2001.

[28] D. E. Williams and F. E. Keith, "Microstructure effects on the response of gas-sensitive resistors based on semiconducting oxides," *Sens. Actuators B*, vol. 70, pp. 214–221, 2000.

[29] N. Bârsan, M. Schweizer-Berberich, and W. Göpel, "Fundamental and practical aspects in the design of nanoscaled SnO_2 gas sensors: A status report," *Fresenius J. Anal. Chem.*, vol. 365, pp. 287–304, 1999.

[30] A. Gurlo, N. Bârsan, M. Ivanovskaya, U. Weimar, and W. Gopel, "In_2O_3 and MoO_3–In_2O_3 thin film semiconductor sensors: Interaction with NO_2 and O_3," *Sens. Actuators B*, vol. 47, pp. 92–99, 1998.

Ismael Jiménez received the degree in physics in 1999 from the University of Barcelona, Barcelona, Spain, where he is currently pursuing the Ph.D. degree at the same university, where he is studying structural and gas sensing properties of metal-oxide nanopowders for applications in gas-sensor devices.

Jordi Arbiol received the degree in physics and the Ph.D. degree from the University of Barcelona, Barcelona, Spain, in 1997 and 2001, respectively. His graduate studies involved applying characterization techniques such as TEM, SEM, AFM, STM, and STS to nanometric metallic oxides.

Albert Cornet received the degree in physics and the Ph.D. degree from the University of Barcelona, Barcelona, Spain, in 1977 and 1982, respecitvely.

Since 1982, he has been with the Physics Faculty of the University of Barcelona, where he has been involved in the research on characterization semiconductor structures, gas sensors, and other advanced materials used in micro or optoelectronic devices. At the present time, he is a Professor with the Electronics Department and a member of the staff of the Electronics Materials and Engineering Laboratory.

Joan Ramon Morante received the Ph.D. degree in physics from the University of Barcelona, Barcelona, Spain, in 1980.

He joined the Department of Applied Physics and Electronics of the University of Barcelona in 1977, and in 1986 he was appointed to Full Professor of electronics in this department. The same year, he founded the Laboratory of Characterization of Materials for Microelectronics (LCMM), and in 1991, he founded the Engineering and Electronic Materials research group (EME), now the Department of Electronics, which he leads. His current research activities and projects are focused on the fields of characterization of electronic materials and processes, micromachined Si-based sensors and actuators, gas sensors, and semiconductors devices. He is the author or coauthor of more than 400 scientific and technical papers.